

## **Effect of a train's cross-sectional shapes on its aerodynamic performance subjected to crosswinds at a windbreak transition**

Zhengwei Chen<sup>1)</sup>, Syeda Anam Hashmi<sup>3)</sup>, \*Tanghong Liu<sup>2)</sup>, Hassan Hemida<sup>4)</sup>

<sup>1), 2)</sup> Key Laboratory of Traffic Safety on Track of Ministry of Education, School of Traffic & Transportation Engineering, Central South University, Changsha 410075, China.

<sup>1)</sup> [gszxczw@csu.edu.cn](mailto:gszxczw@csu.edu.cn) <sup>2)</sup> [lth@csu.edu.cn](mailto:lth@csu.edu.cn)

<sup>3), 4)</sup> Birmingham Centre for Railway Research and Education, School of Civil Engineering, University of Birmingham B15 2TT, UK.

<sup>3)</sup> [sah232@bham.ac.uk](mailto:sah232@bham.ac.uk) <sup>4)</sup> [h.hemida@bham.ac.uk](mailto:h.hemida@bham.ac.uk)

### **ABSTRACT**

Under the influence of strong winds, a windbreak wall is usually built to mitigate the effects of crosswinds. However, due to the effects of different terrains, the windbreak is usually not continuous, and as a result, a right-angle transition might be generated from the flat ground to the cutting position. Consequently, the wind speed has a sudden change around this region. To understand the effect of this transition on the aerodynamic performance of trains, the flows around a train with different cross-section shapes are simulated numerically, and the results are compared and analysed in this transition region.

Keywords: windbreak transition, high-speed train, cross-section shapes, CFD.

### **1. INTRODUCTION**

In China, the Lanzhou–Xinjiang passenger railway is a double line with a total length of about 1777 km. This is the first railway to be built through an area with strong winds (Li, 2012). The windbreak is built along the railway, but a part of the railway line passes through mountainous terrains. Therefore, the windbreak is made discontinuously, which results in many windbreak transition regions between the flat ground/embankment and cuttings. The aerodynamic performance and dynamic index of a vehicle system showed sudden changes and became worse mainly in the position of the discontinuous transition region (Liu D et al., 2018). This phenomenon has an effect

---

<sup>1)</sup> Graduate Student

<sup>3)</sup> Graduate Student

<sup>2)</sup> Professor

<sup>4)</sup> Professor

on both, the passenger comfort as well as the operational safety (Xu et al., 2019). Focusing on this issue and considering a real terrain, Liu T et al. (2018) and Chen et al. (2019) investigated the aerodynamic performance and the dynamic response when a train passes through such transition regions under crosswinds. The studies showed that when the vehicle passes the right-angle transition region, the dynamic parameters strongly vary with the aerodynamic forces, where after the excitation, the dynamic parameters require a long time to return to a stable state. To reduce the effect of this transition on the train aerodynamic performance, the windbreak transition usually is optimised. However, the impact of the cross-sectional shape of the train is not well understood and whether it has any effect on the stability of trains in this region. In the present work, different cross-section shapes of a train are compared in the windbreak transition region to determine which shape is better in terms of the train aerodynamic performance.

## 2. NUMERICAL DETAILS

### 2.1 Model description

Fig. 1 shows the computational model. The train is located on the railway line-2 (RL-2). The railway line-1 (RL-1) is the one close to the windbreak wall. The train height  $h$  is measured from the top of the rail (TOR) and is taken as the reference length. Similar to the wind tunnel testing, the train is stationary and is subjected to crosswind at  $90^\circ$  yaw angle. Only the head car and a half of the second car are considered. Furthermore, the train is located in the region of windbreak transition. As shown in Fig. 2, five different cross-section shapes are studied in the present work. To compare conveniently, the width of the third model,  $W_0=1$ , is taken as the reference value. With the other cross-section areas decreases or increases, the corresponding shapes are named  $W-2=0.85$ ,  $W-1=0.95$ ,  $W+1=1.02$  and  $W+2=1.06$ . The nose shape of the head car is kept unchanged, and only the cross-sectional shape of the car body changes from narrow shape to the round drum shape.

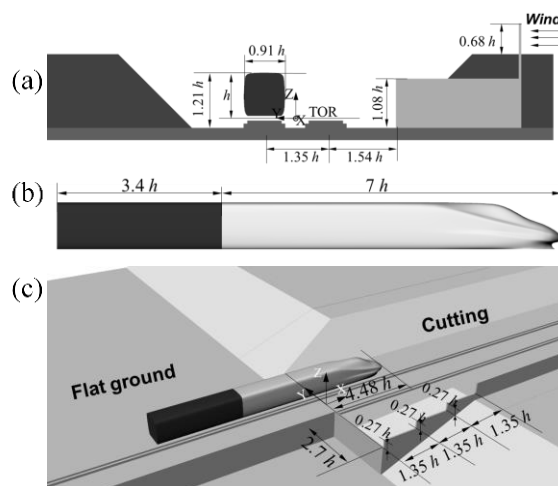
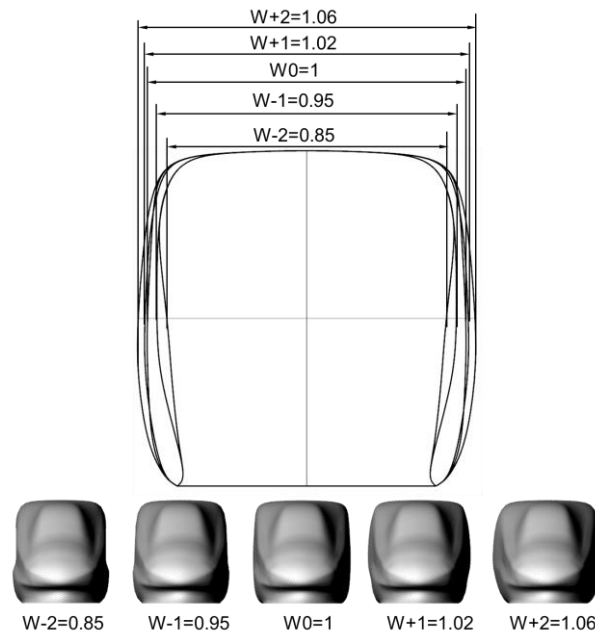


Fig. 1 Computational model: (a) front view, (b) side view of the train, and (c) 3-D view



**Fig. 2** Different cross-section shapes for the train

## 2.2 Numerical method and settings

A 1:25 scaled model is used in the computational analysis. The three-dimensional incompressible unsteady Reynolds averaged Navier–Stokes (URANS) equations and the SST  $k - \omega$  turbulence models (Menter, 1994) are used in this study. The commercial software package Fluent is used, and the governing equations are discretised by the finite volume method (FVM). The convection and diffusion terms are discretised by the second-order upwind scheme, and the time derivative is discretized by the second-order implicit scheme for unsteady flow calculations. The velocity-pressure coupling and solution procedures are based on the Semi-Implicit Method for Pressure Linked Equations (SIMPLEC) algorithm. The time-step,  $\Delta t$ , is  $1 \times 10^{-4}$  s, and the data obtained is for a physical time of 3.0 s. This time allows the flow to pass over the width of the railway more than 20 times. The minimum mesh size is about 0.07 mm, which makes the average  $y^+$  around the model less than 10. According to the ANSYS Fluent Theory Guide (Ansys fluent, 2013), the  $\omega$ -equation can be integrated through the viscous sublayer by using a  $y^+$ -insensitive wall treatment, which blends the viscous sublayer formulation and the logarithmic layer formulation based on  $y^+$ . This formulation is the default for all  $\omega$ -equation based models. The enhanced wall treatment (EWT) is used in this paper to find the shear stress at the first cell close to the wall. This way, the calculations in this paper were feasible. Fig. 3 shows the computational domain, the boundary conditions, and mesh used.

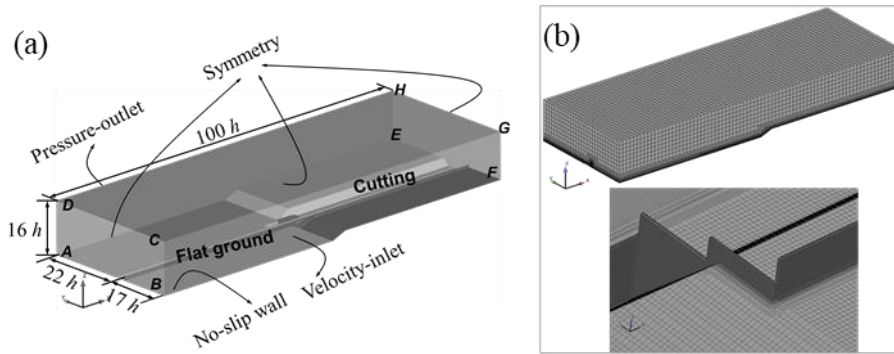


**Fig. 3** Computational domain and mesh: (a) boundary conditions, and (b) mesh

### 3. RESULT DISCUSSIONS

#### 3.1 Aerodynamic forces

The side force coefficient,  $C_y$ , the lift force coefficient,  $C_z$ , and the rolling moment coefficient,  $C_{mx}$ , are discussed in this section. In Eq. (1),  $F_y$ ,  $F_z$ ,  $M_x$  are the side force, lift force and roll moment, respectively. The air density,  $\rho$ , is  $1.225 \text{ kg/m}^3$ , and the wind speed,  $u$ , is  $35 \text{ m/s}$ . The reference area,  $A$ , is the full-scale cross-sectional area and is taken as  $11.22 \text{ m}^2$  and  $l$  is the reference length, which is  $3 \text{ m}$  for a full-scale train.  $C_p$  is the pressure coefficient,  $p$  is the pressure on the train surface, and  $p_0$  is the reference pressure, which is  $0 \text{ pa}$ .

$$C_y = \frac{F_y}{\frac{1}{2}\rho u^2 A}, \quad C_z = \frac{F_z}{\frac{1}{2}\rho u^2 A}, \quad C_{mx} = \frac{M_x}{\frac{1}{2}\rho u^2 A l}, \quad C_p = \frac{p-p_0}{\frac{1}{2}\rho u^2} \quad (1)$$

Fig. 4 shows the aerodynamic coefficients obtained from the different cross-sectional shapes. Due to the head car being located next to the windbreak transition region, the insufficient protection effect of this region leads to the  $C_y$  and  $C_z$  being positive and the  $C_{mx}$  being negative. When the dimensionless width  $W$  increases, the side shape of the car body becomes a drum type, and for the head car, the  $C_y$  and  $C_{mx}$  decrease by 7% and 15%, respectively; but the  $C_z$  increases by 26%.

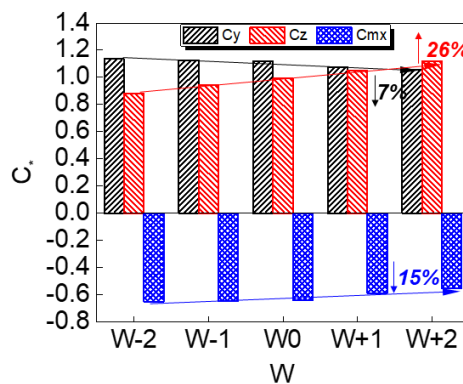


**Fig. 4** The variation of the aerodynamic coefficient with the dimensionless width

### 3.1 Flow structures

Fig. 5 shows the pressure distribution on the head car, which explains why aerodynamic forces change in Fig. 4. As shown in Fig. 5(a) and (b), region A in the windward side (WWS) and region D, F in the leeward side (LWS), where the pressure distributions of shapes W-2 and W+2 are similar. However, for region B, C and E, the surface pressure of W-2 in the WWS is more significant than that of W+2, and the surface pressure of W-2 in the LWS is smaller than that of W+2. Note that the area of region B, C in the WWS is bigger than that of region A, and region E in the LWS is bigger than that of region D and F. Therefore, the side force of W+2 is smaller. In Fig. 5(c) and (d), although the pressure in region G of W+2 is larger than that of W-2, the pressure in region H of W+2 is less than that of W-2, and it can be seen that the region H is dominant at the top position. Furthermore, at the bottom, the pressure distribution of W-2 and W+2 is close to each other, but the bottom area of W+2 is bigger. Combined the top and bottom pressure results, the lift force is larger for the shape of W+2.

Besides, for a better understanding of the effect of cross-sectional shape on the aerodynamic forces, the streamline at  $x=1h$  is shown in Fig. 6. In the WWS, there is a separation point (SP) at the middle height of W-2 but it is at the top position of W+2. The airflow at the upper and lower of SP has an impact and compression effect on the car body of W-2, but for the W+2, the compression effect is less, and the airflow has a smooth motion along the drum sidewall. Fig. 6 shows a vortex V2 generated in the LWS, and the same vortex is constant in size along the width of the cutting in case of W+2. The regularity of vortex V2 in W+2 makes the flow more stable and thus provides less fluctuations in the aerodynamic coefficients. However, the size of V2 beyond the cutting range and it has a suction effect on the airflow that in the LWS of the W-2. Therefore, combined with the flow structures in the WWS and LWS, it can be found the side force of W+2 is smaller. On the other hand, the more airflow enters to the bottom of W+2 leads to a larger lift force than that of W-2.

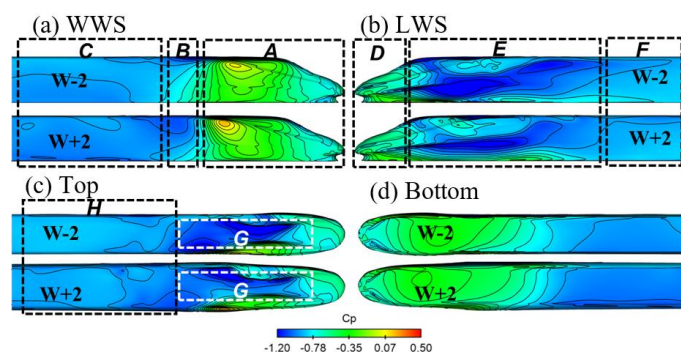
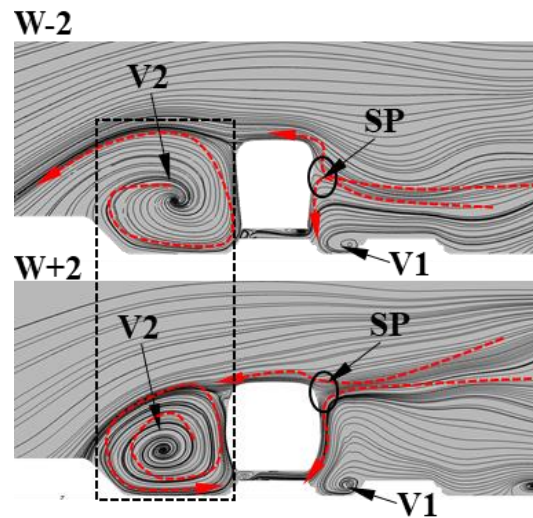


Fig. 5 The pressure distribution on the head car: (a) WWS (b) LWS, (c) top, and (d) bottom surface.



**Fig. 6** The streamlines around the train ( $x=1h$ )

#### 4. CONCLUSIONS

- (1) When the dimensionless width  $W$  increases, the side shape of the car body becomes a drum type, and for the head car, the  $C_y$  and  $C_{mx}$  decrease by 7% and 15%, respectively; but the  $C_z$  increases by 26%.
- (2) The airflow at the upper and lower of SP has an impact and compression effect on the car body of W-2, but for the W+2, the airflow has a smooth motion along the drum sidewall. Due to increased airflow entering the bottom of W+2, this leads to a larger lift force for the W+2.

#### ACKNOWLEDGEMENTS

This work was supported by the National Key R&D Program of China (Grant No. 2016YFB1200504-B-02).

#### REFERENCES

- ANSYS Fluent Theory Guide 15.0. (2013).
- Chen, Z., Liu, T., Li, M., Yu, M., Lu, Z. and Liu, D. (2019), "Dynamic response of railway vehicles under unsteady aerodynamic forces caused by local landforms", *Wind and Structures.*, **29**(3), 149-161.
- Li, K. (2012), "Research on new anti-wind facility of high-speed train in strong wind area", *Journal of Central South University (Science and Technology).*, **43**(2), 756-762.
- Liu, D., Lu, Z., Zhong, M., Cao, T., Chen, D. and Xiong, Y. (2018), "Measurements of car-body lateral vibration induced by high-speed trains negotiating complex terrain sections under strong wind conditions", *Vehicle System Dynamics.*, **56**(2), 173-189.

*The 2020 World Congress on  
Advances in Civil, Environmental, & Materials Research (ACEM20)  
25-28, August, 2020, GECE, Seoul, Korea*

- Liu, T., Chen, Z., Zhou, X. and Zhang, J. (2018), "A CFD analysis of the aerodynamics of a high-speed train passing through a windbreak transition under crosswind", *Engineering Applications of Computational Fluid Mechanics.*, **12**(1), 137-151.
- Menter, F.R. (1994), "Two-equation eddy-viscosity turbulence models for engineering applications", *AIAA Journal.*, **32**(8), 1598-1605.
- Xu, J., Chen, Z.W. and Liu, T.H. (2019), "Experimental and numerical research on the safety of an EMU running on a normal-speed railway line under strong wind", In: *3rd International conference on traffic engineering and transportation system.*, Jiaozuo, China.